THE JOURNAL OF PHYSICAL CHEMISTRY Letters

Letter

Cite This: J. Phys. Chem. Lett. 2019, 10, 3501−3508

pubs.acs.org/JPCL

Detection of the Surface of Crystalline Y_2O_3 Using Direct ^{89}Y Dynamic Nuclear Polarization

Nick J. Brownbill,[†] Daniel Lee,[‡] Gaël De Paëpe,[‡] and Frédéric Blanc*[,†,§]

[†]Department of Chemistry, University of Liverpool, Crown Street, Liverpool L69 7ZD, United Kingdom

[‡]Univ. Grenoble Alpes, CEA, IRIG, MEM, F-38000 Grenoble, France

[§]Stephenson Institute for Renewable Energy, University of Liverpool, Crown Street, Liverpool L69 7ZF, United Kingdom

Supporting Information

ABSTRACT: Nuclei with low gyromagnetic ratio (γ) present a serious sensitivity challenge for nulear magnetic resonance (NMR) spectroscopy. Recently, dynamic nuclear polarization (DNP) has shown great promise in overcoming this hurdle by indirect hyperpolarization (via ^1H) of these low-γ nuclei. Here we show that at a magnetic field of 9.4 T and cryogenic temperature of about 110 K direct DNP of ^{89}Y in a frozen solution of $Y(NO_3)_3$ can offer signal enhancements greater than 80 times using exogeneous trityl OX063 monoradical by satisfying the cross effect magic angle spinning (MAS) DNP mechanism. The large signal enhancement achieved permits ^{89}Y NMR spectra of Y_2O_3 and Gd_2O_3-added Y_2O_3 materials to be obtained quickly (~30 min), revealing a range of surface yttrium hydroxyl groups in addition to the two octahedral yttrium signals of the core. The results open up promises for the observation of low gyromagnetic ratio nuclei and the detection of corresponding surface and (sub-)surface sites.

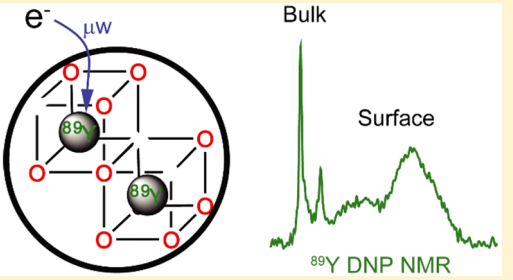

Nuclear magnetic resonance (NMR) spectroscopy is one of the most versatile analytical techniques used to understand the structure and dynamics of solid-state materials. The technique can provide detailed atomic-scale information, making it a widely applied approach across biochemistry, polymer science, battery materials, and many other facets of materials science.[1−3] However, solid-state NMR is impeded by its intrinsic low sensitivity as a result of the combination of the low polarization of nuclei in a magnetic field (also present in liquid-state NMR) and the presence of anisotropic interactions, which significantly broaden the NMR spectra.[2] This limitation is especially pronounced for nuclei with a low gyromagnetic ratio γ (arbitrarily defined as lower than that of ^{15}N at $-27.116\ 10^6$ rad s^{-1} T^{-1}) as the signal-to-noise ratio scales as $\gamma^{5/2}$.

Nuclei with low-γ are involved in a wide range of biological and physical processes:[4,5] for example, magnesium (NMR active nucleus ^{25}Mg) is present in many naturally occurring clays, organic compounds, and oxides;[6] potassium (most NMR-sensitive nucleus ^{39}K) is important in biochemistry and solid-state chemistry;[4] calcium (NMR active nucleus ^{43}Ca) is of great interest due to its presence in biomolecules and other minerals;[7] yttrium (^{89}Y) is of interest, for instance, in pyrochlore ceramic materials where it can be used as a probe for cation disorder.[8]

Many approaches have been taken to improve the NMR sensitivity of solids, perhaps most notably magic angle spinning (MAS), used to average out orientation-dependent interactions that can lead to spectral broadening,[9] and cross-polarization (CP), which can enhance the sensitivity of heteronuclei using the higher polarization of receptive nuclei (e.g., ^1H, ^{19}F).[10] Combining these techniques with dynamic nuclear polarization (DNP)[11−13] has introduced further, and dramatic, enhancements of the NMR signals from solid samples.[14−18] The DNP approach exploits the transfer of the high polarization of unpaired electrons (~660 times larger than ^1H), which are usually added to a sample in the form of stable free radicals[13] or transition metal ions,[19] to nuclei via suitable microwave (μw) irradiation[11,12] followed by their detection. Thanks to numerous developments, including in hardware,[20−24] sample preparation,[13,14] and polarizing agents,[25−29] DNP can yield a boost of NMR sensitivity of multiple orders of magnitude. The MAS DNP approach is typically combined with CP in order to hyperpolarize abundant ^1Hs (or ^2H in isotopically enriched samples)[30] and take advantage of their efficient homonuclear spin diffusion to distribute the polarization[31] before its transfer to the heteronucleus X of interest.

In particular, indirect DNP (i.e., via CP) is becoming an unrivalled method to address the NMR sensitivity issue of low-γ nuclei and has been exploited to probe the local yttrium environment and proton−yttrium connectivity in doped $BaZrO_3$[32] by ^{89}Y NMR, carbonated hydroxyapatite by ^{43}Ca NMR,[33] and silica-supported yttrium−amide complexes by ^{89}Y NMR.[34] These approaches are complementary to those using ^1H detection and very fast MAS for the acquisition of the NMR spectra of low-γ nuclei, as very recently illustrated for

Received: April 25, 2019
Accepted: May 31, 2019
Published: May 31, 2019

DOI: 10.1021/acs.jpclett.9b01185
J. Phys. Chem. Lett. 2019, 10, 3501−3508

^{89}Y, ^{103}Rh, ^{109}Ag, and ^{183}W, offering a significant sensitivity boost compared to standard CP.[35]

However, many solids do not possess protons, therefore ruling out the use of {^{1}H-}X CP and challenging the MAS DNP approach for sensitivity enhancement. One alternative approach can rely on direct transfer of polarization from the radical to the heteronucleus of interest (i.e., direct DNP).[36−41] Unlike in CP, the small homonuclear dipolar coupling of low-γ nuclei limits spin diffusion, rendering the propagation of hyperpolarization from direct DNP throughout the sample extremely inefficient. Nevertheless, it has recently been shown that homonuclear spin diffusion can be used to efficiently propagate DNP into bulk materials containing no protons when exploiting slow spin−lattice relaxation times (e.g., in ^{29}Si, ^{31}P, ^{113}Cd, and ^{119}Sn).[42] However, the spin diffusion coefficient is proportional to γ^2 and is expected to be small for low-γ nuclei (estimated around 2 nm^2 s^{-1} for ^{89}Y in Y_2O_3 based on recent work[42]), and homonuclear spin diffusion might therefore not be effective for low-γ nuclei.

Transition and rare earth metal oxides lacking intrinsic protons find widespread applications in materials science, chemistry, and catalysis. Their NMR investigation has been facilitated by the development of DNP NMR at high magnetic fields, and ^{17}O DNP allows insights into the structure of these materials;[39−41,43,44] however, the DNP NMR detection of the cations themselves has been largely unexplored so far.

In this work, we demonstrate large signal enhancements (ε_{89Y}) for directly polarized ^{89}Y in frozen solutions with both the monoradical trityl OX063[25] ($|\varepsilon_{89Y}| > 80$) and the binitroxide radical AMUPol[28] ($|\varepsilon_{89Y}| > 30$) as sources of polarization. Gains in sensitivity larger than 40 are also demonstrated in Y_2O_3 nanoparticles that are either pristine or Gd_2O_3-added. We show that the approach allows the observation of yttrium hydroxyls and yttria surface sites, as well as those from the bulk, demonstrating its versatility.

Materials Preparation. $Y(NO_3)_3{\cdot}6D_2O$ crystals were prepared by dissolving $Y(NO_3)_3{\cdot}6H_2O$ (Sigma-Aldrich, 99.8%) in a 100-fold weight excess of D_2O (Sigma-Aldrich, 99.9% D) and evaporation of the solvent in air for 24 h.

Y_2O_3 and 0.1% Gd_2O_3-added Y_2O_3 samples were synthesized through a glycine−nitrate combustion route from $Y(NO_3)_3{\cdot}6H_2O$ and $Gd(NO_3)_3{\cdot}6H_2O$ (both Alfa Aesar, 99.9%) and glycine (Alfa Aesar, 99.7%) as starting materials. Stoichiometric ratios of the reactants were mixed in deionized water (5−10 mL) with a nitrate-to-glycine ratio of 2:1. Mixtures were then dehydrated on a hot plate, and autoignition followed. Powders were then ground and fired at 1000 °C for 12 h, pressed into pellets and sintered at 1000 °C for 12 h, and finally slowly cooled to room temperature and finely ground. Both materials were shown to be phase-pure and of similar sized nanoparticles by PXRD (Figure S2).

Powder X-ray Diffraction. Powder X-ray diffraction (PXRD) data were collected in Bragg−Brentano mode on a Panalytical X'Pert Pro diffractometer using monochromated Co Kα1 radiation (λ = 1.7890 Å). The crystallite sizes of Y_2O_3 and 0.1% Gd_2O_3-added Y_2O_3 were determined by Debye−Scherrer analysis and found to be 38.2 ± 10.8 and 37.5 ± 12.9 nm, respectively (see Figure S2).

DNP Sample Preparation. A 5 M yttrium nitrate solution was prepared by dissolving $Y(NO_3)_3{\cdot}6D_2O$ in glycerol-d_8/D_2O/H_2O (6:3:1 volume ratio) containing either 10 mM AMUPol biradical[28] or 40 mM trityl OX063 monoradical (henceforth referred to as trityl).[25] The same amount of the solution (25 μL) was then packed into a 3.2 mm sapphire rotor and closed with a silicone plug and a zirconia drive cap.

Y_2O_3 and 0.1% Gd_2O_3-added Y_2O_3 samples for DNP were prepared by wetness impregnation of finely ground powders (typically 50 mg) with 30 μL of either 10 mM AMUPol biradical or 40 mM trityl in glycerol-d_8/D_2O/H_2O (6:3:1 volume ratio). The same amount of sample was then packed into 3.2 mm sapphire rotors and sealed with zirconia drive caps.

NMR Methods. All DNP NMR experiments were performed on a 9.4 T Bruker Avance III spectrometer operating at 9.4 T and a gyrotron μw source at 263.66 GHz.[22,24] Experiments were recorded with a 3.2 mm HXY triple resonance MAS probe; for experiments with AMUPol[28], the probe was tuned to $\nu_0(^1H)$ = 400.321 MHz with the X channel tuned to $\nu_0(^{13}C)$ = 100.403 MHz and the Y channel tuned to $\nu_0(^{89}Y)$ = 19.700 MHz; for experiments with trityl, the probe was tuned to $\nu_0(^{13}C)$ = 100.725 MHz and $\nu_0(^{89}Y)$ = 16.672 MHz on the X and Y channels, respectively; these configurations correspond to the maximum signal enhancement for each nucleus observed in the MAS DNP magnetic field sweep profiles. All experiments were acquired at a MAS rate of ν_r = 5 kHz and at a sample temperature of T = ∼110 K. ^{1}H pulses and SPINAL-64 decoupling[45] applied during ^{13}C or ^{89}Y detection were performed at a radio frequency (rf) amplitude of 100 kHz. ^{13}C and ^{89}Y directly excited spectra were obtained with a rotor synchronized spin echo sequence with pulses performed at rf amplitudes of 50 and 10 kHz, respectively. {^{1}H-}^{13}C and {^{1}H-}^{89}Y CP experiments were obtained with a 50−100% ^{1}H ramp to 100% ^{13}C/^{89}Y, reaching maxima of 30 and 70 kHz for ^{1}H when matched to ^{13}C at 50 kHz and ^{89}Y at 13 kHz, for a duration of 4 and 10−20 ms, respectively. Recycle delays of 1.3 × $\tau_{DNP}(^1H)$[46] were used for {^{1}H-}X CP experiments, where τ_{DNP} is the measured time constant for the polarization to return to equilibrium after saturation, which was extracted from a saturation recovery experiment with a fit to a stretch exponential function of the form $1 - \exp(-t/\tau_{DNP})^{\beta}$ (where t and β are the variable delays and stretch exponential factor, respectively). The DNP field profiles were recorded by altering the external magnetic field (B_0) using the sweep coil of the Bruker Ascend DNP NMR magnet while keeping the gyrotron μw frequency fixed at 263.66 GHz (^{1}H data with trityl were taken from the literature).[47] All ^{13}C and ^{89}Y MAS NMR spectra recorded in the field profile were obtained with a build-up time of 60 s, and all other directly excited ^{13}C and ^{89}Y spectra were recorded with a build-up time of 120 s. All spectra were collected at the optimal microwave power for signal enhancement. ^{1}H, ^{13}C, and ^{89}Y spectra were referenced to H_2O at 4.8 ppm, the silicone plug at 0 ppm, and the most intense resonance of Y_2O_3 at 330 ppm, respectively. All employed pulse programs are depicted in Figure S1.

The signal enhancement for a particular nucleus ε_n was obtained by scaling the signal recorded in the absence of μw irradiation (μw off) to that with μw (μw on). Where no signal can be obtained without μw irradiation, minimum ε_n values were given by scaling the noise to the μw on signal; this is the case for the ^{13}C and ^{89}Y enhancement values for the frozen solution of $Y(NO_3)_3$ in glycerol-d_8/D_2O/H_2O and for the broad ^{89}Y signals centered at ∼100 ppm for Y_2O_3 and 0.1% Gd_2O_3-added Y_2O_3. All DNP field profile plots were normalized to the maximum signal obtained for the given nucleus using either polarizing agent. The ^{1}H DNP field profile plot was normalized to the maximum enhancement obtained in

DOI: 10.1021/acs.jpclett.9b01185
J. Phys. Chem. Lett. 2019, 10, 3501−3508

this work using data reported in the literature for a frozen glycerol/water sample.[47]

To investigate the DNP mechanism responsible for the nuclear hyperpolarization under given experimental conditions, DNP field profiles were recorded. Figure 1 shows the ^{1}H MAS

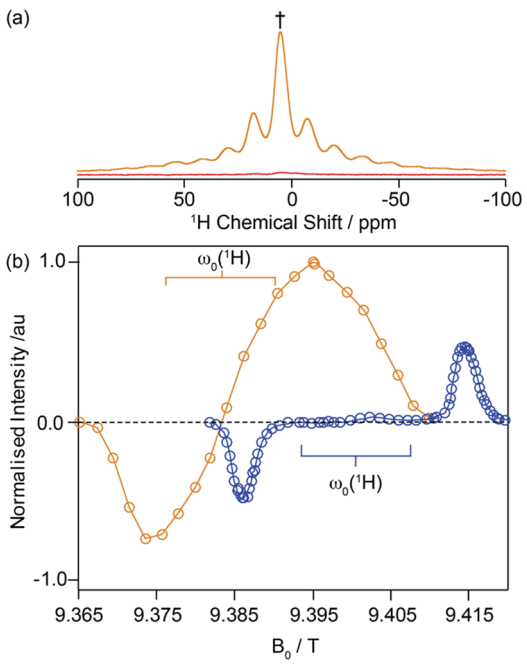

Figure 1. ^{1}H MAS NMR spectra and MAS DNP field profiles for $Y(NO_3)_3$ in solution. (a) ^{1}H MAS DNP NMR spectra of $Y(NO_3)_3$ in a solution of glycerol-d_8/D_2O/H_2O in a 6:3:1 ratio (v/v) with AMUPol biradical as the polarizing agent with μw on (orange) and μw off (red). The dagger (†) denotes the isotropic resonance. (b) ^{1}H MAS DNP field profiles for AMUPol[28] (orange) and trityl[25] (blue, adapted from ref 47). The intensities are normalized to the maximum signal obtained. $\omega_0(^1H)$ is shown centered to the isotropic resonance of the corresponding radicals.

DNP field profiles of 5 M $Y(NO_3)_3$ solution with either AMUPol (10 mM) or trityl (40 mM) as a polarizing agent. The typical profile for the solid effect (SE) mechanism giving ^{1}H enhancement is observed with using the trityl radical (Figure 1b, blue, Table 1),[47] which has a relatively narrow EPR signal, showing the characteristic negative and positive enhancement peaks separated by $2 \times \omega_0(^1H)$ (where $\omega_0(^1H)$ is the ^{1}H Larmor frequency). The SE mechanism is expected as the ^{1}H Larmor frequency (400.321 MHz) at 9.4 T exceeds both the homogeneous (δ)[25] and inhomogeneous ($\Delta \approx 90$ MHz at 9.4 T,[48] extrapolated from a value of 50 MHz at 5 T[49] using the linear relationship between width and field strength for trityl[50]) EPR line widths of trityl, satisfying the selection condition of this mechanism

$$\omega_0(^1H) > \delta, \Delta \quad (1)$$

Figure 1b (orange) shows the ^{1}H field profile with AMUPol as a polarizing agent and is characteristic of the CE MAS DNP mechanism. AMUPol does not fulfill the condition given in eq 1 as the inhomogeneous EPR line width Δ (>600 MHz for the related TOTAPOL)[26] exceeds the ^{1}H nuclear Larmor frequency, and AMUPol instead satisfies the CE condition

$$\Delta > \omega_0(^1H) > \delta \quad (2)$$

The largest enhancement for ^{1}H with AMUPol was observed at the maximum positive enhancement (B_0 = 9.395 T) and is ~1.2 times larger than the maximum negative signal enhancement, typical for water-soluble binitroxide radicals.[26]

A comparison of the ^{13}C MAS DNP field profiles for AMUPol and trityl at 110 K is given in Figure 2. The field profile for ^{13}C, a moderate γ nucleus, with AMUPol shows the typical characteristics of the CE mechanism as anticipated as Δ greatly exceeds $\omega_0(^{13}C)$. At the optimum negative position (B_0 = 9.380 T) a maximum signal enhancement of $|\varepsilon_{^{13}C}| \geq 58$ is obtained (Table 1). The ^{13}C MAS DNP field profile for trityl

Table 1. Enhancement Values and Build-up Times for ^{1}H, ^{13}C, and ^{89}Y Nuclei in 5 M $Y(NO_3)_3$ Solution in a 6:3:1 (v/v) Glycerol-d_8/D_2O/H_2O Solution for AMUPol or Trityl 9.4 T and 110 K

radical	nucleus	DNP mechanism	$\lvert\varepsilon_n\rvert$	τ_{DNP} (s)
AMUPol (10 mM)	^{1}H	CE	60	7.9 ± 0.2
	^{13}C	CE	>58	>2300
	^{89}Y	CE	>30	>2200
trityl (40 mM)	^{1}H[a]	SE	29	*b*
	^{13}C	CE/SE	>35	*b*
	^{89}Y	CE	>80	>2600

[a]Values extracted from ref 47. [b]These values were not recorded.

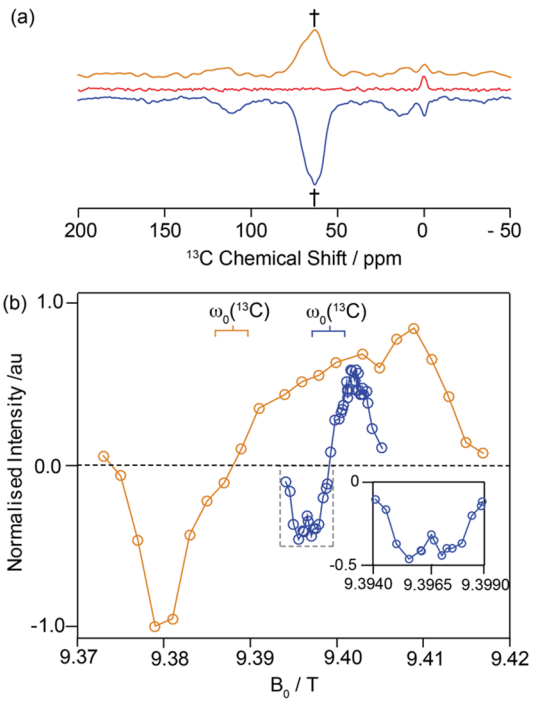

Figure 2. ^{13}C MAS NMR spectra and MAS DNP field profiles for $Y(NO_3)_3$ in solution. (a) ^{13}C MAS DNP NMR spectra of $Y(NO_3)_3$ in a solution of glycerol-d_8/D_2O/H_2O in a 6:3:1 ratio (v/v) with μw on for trityl (blue) and AMUPol (orange) as the polarizing agent and with μw off (red). The resonance at 0 ppm corresponds to the silicone plug, and the dagger (†) denotes the isotropic resonances (not resolved) of glycerol. (b) ^{13}C MAS DNP field profiles for AMUPol[28] (orange) and trityl[25] (blue) with the inset showing the double minimum observed for trityl. The intensities are normalized to the maximum signal obtained. $\omega_0(^{13}C)$ is shown centered to the isotropic resonance of the corresponding radicals.

DOI: 10.1021/acs.jpclett.9b01185
J. Phys. Chem. Lett. 2019, 10, 3501−3508

shows a maximum signal ($\varepsilon_{13C} \geq 35$) at the positive maximum (B_0 = 9.403 T) and suggests the presence of the CE mechanism (Table 1, Figure 2b), as has previously been reported at 3.4 T[51] and, recently, at 14.1 T.[52] We note that the absence of NMR signal without DNP enhancement for ^{13}C (and ^{89}Y; see below) prohibits exploitation of the more comprehensive analysis of signal enhancements recently discussed in the literature.[21,31,48,53−55]

The double minimum observed for ^{13}C (Figure 2b, inset) with trityl is indicative of a possible SE contribution to the MAS DNP field profile, which is due to the similar magnitude of the ^{13}C Larmor frequency (100.19 MHz) and the inhomogeneous EPR line width (~90 MHz at 9.4 T; see above). This dual contribution of CE and SE in the hyperpolarization of ^{13}C with trityl highlights the suboptimal CE polarization transfer when Δ is of the same order of magnitude as the nuclear Larmor frequency ($\omega_0(^{13}C)$), resulting in substantially lower overall signal gain for trityl versus AMUPol in this case (Figure 2 and Table 1). It has been reported that radical modification by binding a nitroxide moiety such as TEMPO to a trityl radical can increase the efficiency of this CE character; however, this is beyond the scope of the work reported here.[48,56]

The DNP-enhanced ^{89}Y MAS NMR spectra of $Y(NO_3)_3$ in glycerol-d_8/D_2O/H_2O (6:3:1 volume ratio) (Figure 3a) show two poorly resolved resonances that have previously been assigned[32,57,58] to free $Y(aq)^{3+}$ ions (at −20 ppm) and complex $[Y(glycerol)]^{3+}$ (at 20 ppm) in frozen solution. The ^{89}Y spectrum of $Y(NO_3)_3$ shows a substantially greater maximum enhancement for trityl ($|\varepsilon_{89Y}| > 80$) than AMUPol ($|\varepsilon_{89Y}| > 30$)

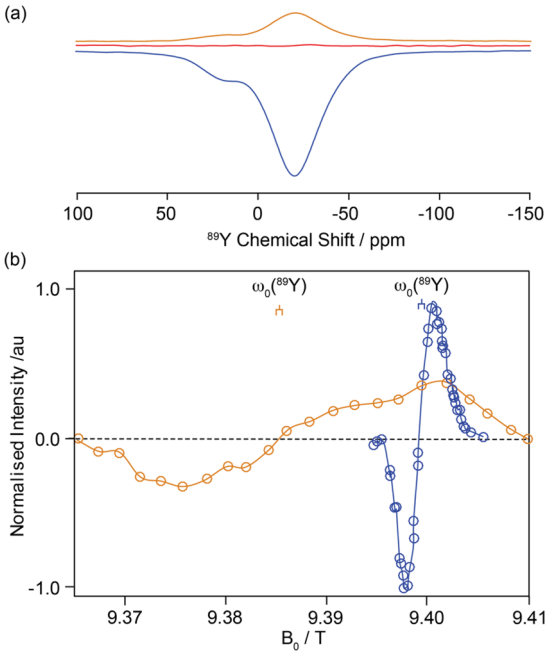

Figure 3. ^{89}Y MAS NMR spectra and MAS DNP field profiles for $Y(NO_3)_3$ in solution. (a) ^{89}Y MAS DNP NMR spectra of $Y(NO_3)_3$ in a solution of glycerol-d_8/D_2O/H_2O in a 6:3:1 ratio (v/v) with μw on for trityl (blue) and AMUPol (orange) and μw off (red). Only the isotropic resonances are shown. (b) ^{89}Y MAS DNP field profiles for binitroxide radical AMUPol[28] (orange) and trityl[25] (blue). The intensities are normalized to the maximum signal obtained. $\omega_0(^{89}Y)$ is shown centered to the isotropic resonance of the corresponding radicals.

(see below for further discussion on these values). The ^{89}Y τ_{DNP} was of the same order of magnitude for either AMUPol or trityl for CE MAS DNP (Table 1), and because all ^{89}Y spectra were recorded with a short recycle delay of 120 s, trityl showed a significant benefit compared to AMUPol for time-efficient signal enhancement, i.e., overall NMR sensitivity.

Both ^{89}Y MAS DNP field profiles of $Y(NO_3)_3$ in solution with AMUPol and trityl as polarizing agents (Figure 3b) showed the typical CE line shapes, consistent with both radicals satisfying eq 2 due to the small ^{89}Y Larmor frequency (19.67 MHz) compared to the inhomogeneous EPR line widths Δ. As has been previously reported for ^{17}O at 5 T,[40] the CE condition is met sufficiently using trityl, and the resulting polarization transfer can produce significantly larger MAS DNP enhancements than those when using a binitroxide polarizing agent with a broader EPR line (such as AMUPol). This is in part a result of the long electron spin relaxation times of trityl compared to those of the employed binitroxide, as well as the more efficient energy level (anti)crossings responsible for MAS DNP with a narrow-line radical.[48] Here, we use AMUPol, which has been shown[28] to have longer spin relaxation times and to result in 3−4 times the DNP enhancement compared to the TOTAPOL binitroxide polarizing agent used in the ^{17}O work at 5 T.[40] Importantly, Figure 3 shows that, even though AMUPol is a preferred binitroxide for CE MAS DNP, trityl is in fact superior for direct MAS DNP of low-γ nuclei.

Notably, the maximum DNP enhancement for ^{89}Y with AMUPol was obtained on the positive enhancement side of the field profile, whereas for trityl the maximum signal gain was obtained on the negative enhancement side (~1.1 times greater than the positive maximum). All directly polarized ^{89}Y MAS DNP NMR spectra with trityl were subsequently recorded at this field position (B_0 = 9.3975 T) and, as such, are plotted with negative phase (Figures 3−5).

It is important to note the potential influence of nuclear depolarization[59] on the reported enhancement values. In the absence of μw irradiation and in the presence of CE matching under MAS conditions, polarization can be transferred from a nucleus to the two electron spins in a reverse DNP-type process. This occurs when the polarization of the nucleus is greater than the difference in polarization between the two electron spins.[59,60] Therefore, the enhancement ratio, ε_n, can be larger than the nuclear polarization gain when compared to thermal Boltzmann equilibrium, and thus, care should be taken when evaluating DNP performance.

Nuclear depolarization has currently been observed for only ^1H and ^{13}C, but it is theoretically possible for all nuclei.[59] Here, the ^{89}Y NMR sensitivity in the absence of μw irradiation is too small to perform a detailed analysis of the induced nuclear depolarization (and a comprehensive analysis of signal enhancements).[21,31,48,53−55] Because the CE matching condition is met for ^{89}Y for both AMUPol and trityl, it could be expected that the nuclear depolarization is substantial and accordingly that the quoted enhancement values (ε_{89Y}) may not truly represent the gain in nuclear polarization compared to Boltzmann equilibrium, $\varepsilon_{89Y,Boltz}$. Nevertheless, in the presence of μw irradiation, the ratio of the maximum absolute signal to the minimum (nonzero) absolute signal found from the MAS DNP field profile (Figure 3) gives the minimum $\varepsilon_{89Y,Boltz}$; therefore, for AMUPol, $|\varepsilon_{89Y,Boltz}| > 30$, and for trityl, $|\varepsilon_{89Y,Boltz}| > 80$. Furthermore, because these are both obtained in the presence of μw irradiation, it can be safely concluded

DOI: 10.1021/acs.jpclett.9b01185
J. Phys. Chem. Lett. 2019, 10, 3501−3508

that trityl is more efficient for direct ^{89}Y CE MAS DNP than AMUPol at 9.4 T using moderate MAS rates (~5 kHz).

We then turned our attention to crystalline solid materials and targeted Y_2O_3 due to interest in this phase as semiconductors, as a source of yttrium for chemical doping, or for surface treatment.[61] It is well-known that adding a small amount of paramagnetic metal oxide Gd_2O_3 circumvents the extremely long spin−lattice relaxation times T_1 of ^{89}Y in Y_2O_3[62] by decreasing them and is verified experimentally (room temperature T_1 > 3 h for Y_2O_3[62] vs ~3 min in 0.1% Gd_2O_3-added Y_2O_3 for the 330 ppm signal[63]). This allows acquisition of ^{89}Y NMR spectra in the 0.1% Gd_2O_3-added Y_2O_3 phase with good signal-to-noise in 30 min and shows the two characteristic peaks of Y_2O_3 at 330 and 287 ppm in a 3 to 1 ratio, respectively (Figure 4a, red), both sites having a similar

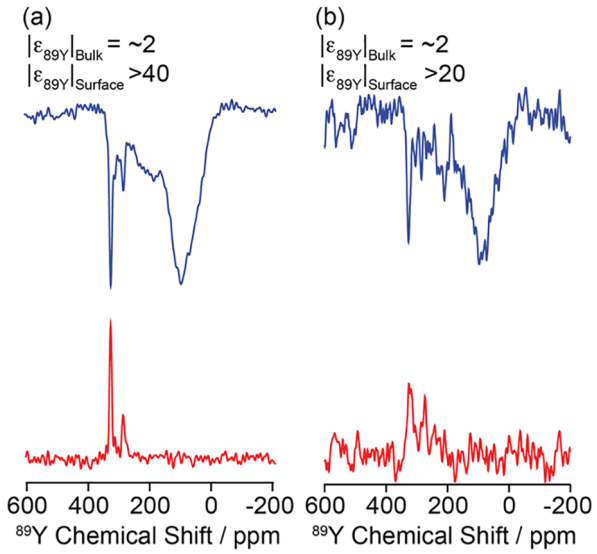

Figure 4. Direct ^{89}Y DNP-enhanced MAS NMR spectra of (a) 0.1% Gd_2O_3-added Y_2O_3 and (b) Y_2O_3, recorded with μw on (blue) and μw off (red). All NMR data were recorded with recycle delays of 120 s and trityl as a polarizing agent at the negative maximum of the field profile (B_0 = 9.3975 T).

DNP build-up time τ_{DNP} (vide infra and Figures 5a and S3). These resonances are typical of the bulk of yttria[63] and correspond to the two octahedral yttrium sites that have 24:8 occupancies in the cubic bixbyte structure (space group *Ia*3) in Y_2O_3.[64] It is possible to observe these signals in pristine Y_2O_3 in the same experimental time (Figure 4b, red) without DNP, albeit with much worse signal-to-noise than that for Gd_2O_3-added Y_2O_3 due to the shortening of the T_1 times by the paramagnetic doping in the latter phase (see above).

The bulk ^{89}Y signals in either 0.1% Gd_2O_3-added Y_2O_3 or pristine Y_2O_3 are barely enhanced by ^{89}Y direct DNP, as revealed by comparing the spectra with and without μw (Figure 4, blue and red, respectively). Note that the two ^{89}Y NMR signals are inverted in the μw on experiment (versus the spectra without μw irradiation), confirming that these sites are indeed hyperpolarized by DNP. More importantly, in addition to these two narrow peaks, two broad resonances centered at approximately 200 and 100 ppm and spanning ~300 ppm are now also clearly observed in both 0.1% Gd_2O_3-added Y_2O_3 and Y_2O_3 and are tentatively assigned to surface sites (vide infra).

Figure 5a plots the direct ^{89}Y MAS DNP build-up curves for surface and bulk sites after saturation in 0.1% Gd_2O_3-added

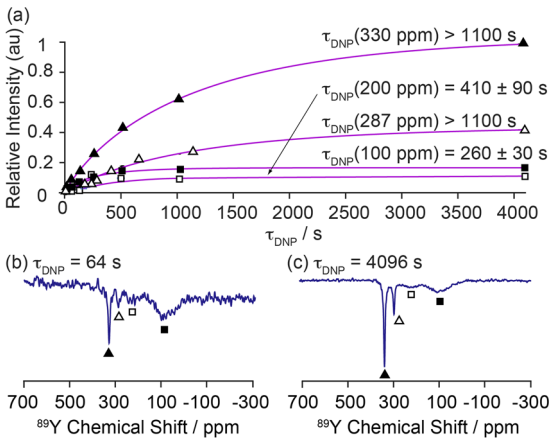

Figure 5. ^{89}Y hyperpolarization build-up and direct ^{89}Y DNP-enhanced MAS NMR spectra of 0.1% Gd_2O_3-added Y_2O_3 with trityl polarizing agent. (a) Fitted build-up curves of the bulk ^{89}Y (330 ppm, filled triangles; 287 ppm, hollow triangles) and surface ^{89}Y sites (~200 ppm, hollow squares; ~100 ppm, filled squares) of 0.1% Gd_2O_3-added Y_2O_3. The curves in purple are fit to the data using a stretch exponential function (see the experimental discussion). The ^{89}Y MAS NMR spectra recorded at τ_{DNP} = (b) 64 and (c) 4096 s are also given for comparison of relative peak intensities.

Y_2O_3, from which the DNP build-up times, τ_{DNP}, can be extracted. While the full build-up is well captured for the ~200 and ~100 ppm sites, yielding polarization times, τ_{DNP}, on the order of 410 ± 90 and 260 ± 30 s, respectively, a hyperpolarization plateau could not be reached (in a time-efficient manner) for the Y_2O_3 bulk sites at 330 and 287 ppm. This is due to the long build-up time, in excess of 15 min for these sites, which is consistent with the T_1 times for crystalline Y_2O_3.[62] The shorter τ_{DNP} of the sites at ~200 and ~100 ppm compared to that of the yttrium bulk site likely indicates a lower degree of order and/or the presence of additional relaxation mechanisms such as a closer proximity to paramagnetic centers (e.g., trityl radical) or dipolar couplings to protons (e.g., yttrium hydroxyls;[5,65] see below), all demonstrating that these resonances arise from surface sites. Consequently, at short τ_{DNP}, the broad surface sites are the dominant feature of the spectrum (Figure 5b), with small contributions from the narrow bulk resonances.

DNP-enhanced {^{1}H-}X CP MAS NMR of materials without intrinsic protons prepared by wetness impregnation with nonsolvents containing protons has been shown to provide surface-selective signal enhancement.[66] Figure 6 shows the DNP-enhanced {^{1}H-}^{89}Y CP MAS NMR spectra of both 0.1% Gd_2O_3-added Y_2O_3 and Y_2O_3 materials recorded under the optimum ^{1}H CE MAS DNP matching condition with AMUPol. In both cases, the dominant resonances are those centered at ~200 and ~100 ppm, leading to the confirmation of their assignments as surface sites, specifically to yttrium hydroxyl Y(OH) sites.[5,65] The ^{89}Y resonance of $Y(OH)_3$ appears at 66 ppm, upfield from Y_2O_3 (at 330 and 287 ppm), and as such, a range of inhomogeneously broadened Y(OH) surface sites resonating between 0 and 300 ppm are consistent with yttrium centers being bound to one (at ~200 ppm) or two hydroxyl groups (at ~100 ppm) on the surface of Y_2O_3. Note that the broadening does not stem from the proximity to Gd^{3+} because the broad Y(OH) surface peaks are also observed in the undoped Y_2O_3 (Figure 4b). A third narrower resonance is observed in the {^{1}H-}^{89}Y CP spectrum

DOI: 10.1021/acs.jpclett.9b01185
J. Phys. Chem. Lett. 2019, 10, 3501−3508

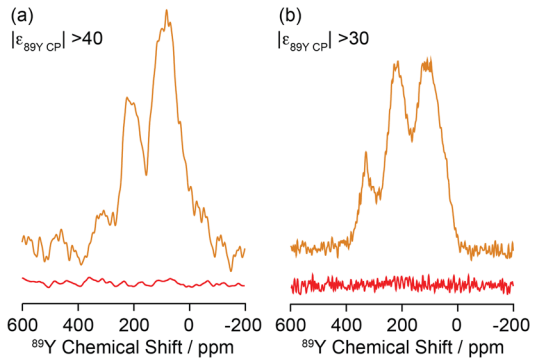

Figure 6. DNP-enhanced $\{^1H\text{-}\}^{89}Y$ CP MAS NMR spectra of yttrium oxides. (a) 0.1% Gd_2O_3-added Y_2O_3 with a CP contact time of 8 ms and (b) Y_2O_3 with a contact time of 20 ms, recorded with μw on (orange) and μw off (red). Note that fewer scans were collected in (b). All $\{^1H\text{-}\}^{89}Y$ CP MAS NMR spectra were recorded with AMUPol at the positive maximum of the ^1H CE (B_0 = 9.395 T).

of pristine Y_2O_3 (Figure 6b) at around 330 ppm, which is likely signal from bulk ^{89}Y. This site is largely enhanced by the long CP contact time (20 ms) that allows some hyperpolarization to penetrate into the bulk of the nanoparticles. This peak is less pronounced, but still observed, in the DNP-enhanced $\{^1H\text{-}\}^{89}Y$ CP MAS NMR spectrum of 0.1% Gd_2O_3-added Y_2O_3 (Figure 6a) and results from a combination of shorter CP contact time (8 ms) used to record this CP spectrum and shorter rotating frame longitudinal relaxation times ^1H $T_{1\rho}$ (due to the presence of Gd_2O_3).

We have demonstrated that it is possible to hyperpolarize low-γ ^{89}Y efficiently in the solid state by directly transferring polarization from electron spins in exogenous radicals, without requiring nearby proton spins. CE MAS DNP with trityl OX063 monoradical yields significant signal enhancement ($|\varepsilon_{89Y}| > 80$), larger than that observed with AMUPol biradical ($|\varepsilon_{89Y}| > 30$) for a frozen solution of $Y(NO_3)_3$. This approach was then employed to interrogate Y_2O_3, and comparison of DNP-enhanced ^{89}Y spectra obtained with and without ^1H CP reveals the presence of a range of yttrium hydroxyl sites at the surface of Y_2O_3. This was possible for both the Gd_2O_3-added and, notably, the unmodified Y_2O_3. This work demonstrates that DNP is a highly viable approach to facilitate the analysis of the atomic-scale environments of low-γ nuclei in the absence of protons in a time-efficient manner without additional modification of materials.

■ ASSOCIATED CONTENT

Supporting Information

The Supporting Information is available free of charge on the ACS Publications website at DOI: 10.1021/acs.jpclett.9b01185.

Details of NMR experiments used, PXRD, and additional figures showing DNP MAS NMR, Hahn echo sequences, PXRD patterns, and fitted build-up curves (PDF)

■ AUTHOR INFORMATION

Corresponding Author

*E-mail: frederic.blanc@liverpool.ac.uk.

ORCID

Gaël De Paëpe: 0000-0001-9701-3593

Frédéric Blanc: 0000-0001-9171-1454

Funding

Financial support from the EPSRC for a Doctoral Training Studentship (to N.J.B.) and Grant EP/M00869X/1 (to F.B.) as well as from the French National Research Agency (ANR-12-BS08-0016-01, ANR-11-LABX-0003-01, and RTB) and the European Research Council (ERC-CoG- 2015, No. 682895) (to G.D.P.).

Notes

The authors declare no competing financial interest.

The experimental data are provided as a supporting dataset from the University of Liverpool Data Catalogue portal at http://dx.doi.org/10.17638/datacat.liverpool.ac.uk/762.

■ ACKNOWLEDGMENTS

N.J.B. thanks Kenneth K. Inglis for valuable technical support with PXRD measurements.

■ REFERENCES

(1) Brown, S. P.; Spiess, H. W. Advanced Solid-State NMR Methods for the Elucidation of Structure and Dynamics of Molecular, Macromolecular, and Supramolecular Systems. *Chem. Rev.* **2001**, *101*, 4125−4155.

(2) Laws, D. D.; Bitter, H.-M. L.; Jerschow, A. Solid-State NMR Spectroscopic Methods in Chemistry. *Angew. Chem., Int. Ed.* **2002**, *41*, 3096−3129.

(3) Blanc, F.; Copéret, C.; Lesage, A.; Emsley, L. High Resolution Solid State NMR Spectroscopy in Surface Organometallic Chemistry: Access to Molecular Understanding of Active Sites of Well-Defined Heterogeneous Catalysts. *Chem. Soc. Rev.* **2008**, *37*, 518−526.

(4) Smith, M. E. Recent Progress in Solid-State NMR of Low-Gamma Nuclei. *Annu. Rep. NMR Spectrosc.* **2001**, *43*, 121−175.

(5) MacKenzie, K. J. D.; Smith, M. E. *Multinuclear Solid-State NMR of Inorganic Materials*; Pergamon Press: Oxford, 2002.

(6) Freitas, J. C. C.; Smith, M. E. Recent Advances in Solid-State ^{25}Mg NMR Spectroscopy. *Annu. Rep. NMR Spectrosc.* **2012**, *75*, 25−114.

(7) Bryce, D. L. Calcium Binding Environments Probed by ^{43}Ca NMR Spectroscopy. *Dalt. Trans.* **2010**, *39*, 8593−8602.

(8) Ashbrook, S. E.; Dawson, D. M. Exploiting Periodic First-Principles Calculations in NMR Spectroscopy of Disordered Solids. *Acc. Chem. Res.* **2013**, *46*, 1964−1974.

(9) Andrew, E. R.; Bradbury, A.; Eades, R. G. Nuclear Magnetic Resonance Spectra from a Crystal Rotated at High Speed. *Nature* **1958**, *182*, 1659−1659.

(10) Pines, A.; Gibby, M. G.; Waugh, J. S. Proton-Enhanced Nuclear Induction Spectroscopy ^{13}C Chemical Shielding Anisotropy in Some Organic Solids. *Chem. Phys. Lett.* **1972**, *15*, 373−376.

(11) Overhauser, A. W. Polarization of Nuclei in Metals. *Phys. Rev.* **1953**, *92*, 411−415.

(12) Carver, T. R.; Slichter, C. P. Experimental Verification of the Overhauser Nuclear Polarization Effect. *Phys. Rev.* **1956**, *102*, 975−980.

(13) Hall, D. A.; Maus, D. C.; Gerfen, G. J.; Inati, S. J.; Becerra, L. R.; Dahlquist, F. W.; Griffin, R. G. Polarization-Enhanced NMR Spectroscopy of Biomolecules in Frozen Solution. *Science* **1997**, *276*, 930−932.

(14) Lesage, A.; Lelli, M.; Gajan, D.; Caporini, M. A.; Vitzthum, V.; Miéville, P.; Alauzun, J.; Roussey, A.; Thieuleux, C.; Mehdi, A.; Bodenhausen, G.; Copéret, C.; Emsley, L. Surface Enhanced NMR Spectroscopy by Dynamic Nuclear Polarization. *J. Am. Chem. Soc.* **2010**, *132*, 15459−15461.

(15) Ni, Q. Z.; Daviso, E.; Can, T. V.; Markhasin, E.; Jawla, S. K.; Swager, T. M.; Temkin, R. J.; Herzfeld, J.; Griffin, R. G. High Frequency Dynamic Nuclear Polarization. *Acc. Chem. Res.* **2013**, *46*, 1933−1941.

(16) Rossini, A. J.; Zagdoun, A.; Lelli, M.; Lesage, A.; Copéret, C.; Emsley, L. Dynamic Nuclear Polarization Surface Enhanced NMR Spectroscopy. *Acc. Chem. Res.* **2013**, *46*, 1942−1951.
(17) Lee, D.; Hediger, S.; De Paëpe, G. Is Solid-State NMR Enhanced by Dynamic Nuclear Polarization? *Solid State Nucl. Magn. Reson.* **2015**, *66*−*67*, 6−20.
(18) Thankamony, A. S. L.; Wittmann, J. J.; Kaushik, M.; Corzilius, B. Dynamic Nuclear Polarization for Sensitivity Enhancement in Modern Solid-State NMR. *Prog. Nucl. Magn. Reson. Spectrosc.* **2017**, *102*−*103*, 120−195.
(19) Corzilius, B.; Smith, A. A.; Barnes, A. B.; Luchinat, C.; Bertini, I.; Griffin, R. G. High-Field Dynamic Nuclear Polarization with High-Spin Transition Metal Ions. *J. Am. Chem. Soc.* **2011**, *133*, 5648−5651.
(20) Becerra, L. R.; Gerfen, G. J.; Temkin, R. J.; Singel, D. J.; Griffin, R. G. Dynamic Nuclear Polarization with a Cyclotron Resonance Maser at 5 T. *Phys. Rev. Lett.* **1993**, *71*, 3561−3564.
(21) Thurber, K. R.; Yau, W.-M.; Tycko, R. Low-Temperature Dynamic Nuclear Polarization at 9.4 T with a 30 MW Microwave Source. *J. Magn. Reson.* **2010**, *204*, 303−313.
(22) Rosay, M.; Tometich, L.; Pawsey, S.; Bader, R.; Schauwecker, R.; Blank, M.; Borchard, P. M.; Cauffman, S. R.; Felch, K. L.; Weber, R. T.; Temkin, R. J.; Griffin, R. G.; Maas, W. E. Solid-State Dynamic Nuclear Polarization at 263 GHz: Spectrometer Design and Experimental Results. *Phys. Chem. Chem. Phys.* **2010**, *12*, 5850−5860.
(23) Bouleau, E.; Saint-Bonnet, P.; Mentink-Vigier, F.; Takahashi, H.; Jacquot, J.-F.; Bardet, M.; Aussenac, F.; Purea, A.; Engelke, F.; Hediger, S.; Lee, D.; De Paëpe, G. Pushing NMR Sensitivity Limits Using Dynamic Nuclear Polarization with Closed-Loop Cryogenic Helium Sample Spinning. *Chem. Sci.* **2015**, *6*, 6806−6812.
(24) Rosay, M.; Blank, M.; Engelke, F. Instrumentation for Solid-State Dynamic Nuclear Polarization with Magic Angle Spinning NMR. *J. Magn. Reson.* **2016**, *264*, 88−98.
(25) Reddy, T. J.; Iwama, T.; Halpern, H. J.; Rawal, V. H. General Synthesis of Persistent Trityl Radicals for EPR Imaging of Biological Systems. *J. Org. Chem.* **2002**, *67*, 4635−4639.
(26) Song, C.; Hu, K.-N.; Joo, C.-G.; Swager, T. M.; Griffin, R. G. TOTAPOL: A Biradical Polarizing Agent for Dynamic Nuclear Polarization Experiments in Aqueous Media. *J. Am. Chem. Soc.* **2006**, *128*, 11385−11390.
(27) Zagdoun, A.; Casano, G.; Ouari, O.; Schwarzwälder, M.; Rossini, A. J.; Aussenac, F.; Yulikov, M.; Jeschke, G.; Copéret, C.; Lesage, A.; Tordo, P.; Emsley, L. Large Molecular Weight Nitroxide Biradicals Providing Efficient Dynamic Nuclear Polarization at Temperatures up to 200 K. *J. Am. Chem. Soc.* **2013**, *135*, 12790−12797.
(28) Sauvée, C.; Rosay, M.; Casano, G.; Aussenac, F.; Weber, R. T.; Ouari, O.; Tordo, P. Highly Efficient, Water-Soluble Polarizing Agents for Dynamic Nuclear Polarization at High Frequency. *Angew. Chem.* **2013**, *125*, 11058−11061.
(29) Mentink-Vigier, F.; Marin-Montesinos, I.; Jagtap, A. P.; Halbritter, T.; van Tol, J.; Hediger, S.; Lee, D.; Sigurdsson, S. T.; De Paëpe, G. Computationally Assisted Design of Polarizing Agents for Dynamic Nuclear Polarization Enhanced NMR: The AsymPol Family. *J. Am. Chem. Soc.* **2018**, *140*, 11013−11019.
(30) Maly, T.; Andreas, L. B.; Smith, A. A.; Griffin, R. G. ^{2}H-DNP-Enhanced ^{2}H-^{13}C Solid-State NMR Correlation Spectroscopy. *Phys. Chem. Chem. Phys.* **2010**, *12*, 5872−5878.
(31) Rossini, A. J.; Zagdoun, A.; Hegner, F.; Schwarzwälder, M.; Gajan, D.; Copéret, C.; Lesage, A.; Emsley, L. Dynamic Nuclear Polarization NMR Spectroscopy of Microcrystalline Solids. *J. Am. Chem. Soc.* **2012**, *134*, 16899−16908.
(32) Blanc, F.; Sperrin, L.; Lee, D.; Dervisoglu, R.; Yamazaki, Y.; Haile, S. M.; De Paëpe, G.; Grey, C. P. Dynamic Nuclear Polarization NMR of Low Gamma Nuclei: Structural Insights into Hydrated Yttrium-Doped $BaZrO_3$. *J. Phys. Chem. Lett.* **2014**, *5*, 2431−2436.
(33) Lee, D.; Leroy, C.; Crevant, C.; Bonhomme-Coury, L.; Babonneau, F.; Laurencin, D.; Bonhomme, C.; De Paëpe, G. Interfacial Ca^{2+} Environments in Nanocrystalline Apatites Revealed by Dynamic Nuclear Polarization Enhanced ^{43}Ca NMR Spectroscopy. *Nat. Commun.* **2017**, *8*, 14104.
(34) Delley, M. F.; Lapadula, G.; Núñez-Zarur, F.; Comas-Vives, A.; Kalendra, V.; Jeschke, G.; Baabe, D.; Walter, M. D.; Rossini, A. J.; Lesage, A.; Emsley, L.; Maury, O.; Copéret, C. Local Structures and Heterogeneity of Silica-Supported M(III) Sites Evidenced by EPR, IR, NMR, and Luminescence Spectroscopies. *J. Am. Chem. Soc.* **2017**, *139*, 8855−8867.
(35) Venkatesh, A.; Ryan, M. J.; Biswas, A.; Boteju, K. C.; Sadow, A. D.; Rossini, A. J. Enhancing the Sensitivity of Solid-State NMR Experiments with Very Low Gyromagnetic Ratio Nuclei with Fast Magic Angle Spinning and Proton Detection. *J. Phys. Chem. A* **2018**, *122*, 5635−5643.
(36) Maly, T.; Miller, A.-F.; Griffin, R. G. In Situ High-Field Dynamic Nuclear Polarization-Direct and Indirect Polarization of ^{13}C Nuclei. *ChemPhysChem* **2010**, *11*, 999−1001.
(37) Lafon, O.; Rosay, M.; Aussenac, F.; Lu, X.; Trébosc, J.; Cristini, O.; Kinowski, C.; Touati, N.; Vezin, H.; Amoureux, J.-P. Beyond the Silica Surface by Direct Silicon-29 Dynamic Nuclear Polarization. *Angew. Chem., Int. Ed.* **2011**, *50*, 8367−8370.
(38) Lee, D.; Takahashi, H.; Thankamony, A. S. L.; Dacquin, J.-P.; Bardet, M.; Lafon, O.; De Paëpe, G. Enhanced Solid-State NMR Correlation Spectroscopy of Quadrupolar Nuclei Using Dynamic Nuclear Polarization. *J. Am. Chem. Soc.* **2012**, *134*, 18491−18494.
(39) Blanc, F.; Sperrin, L.; Jefferson, D. A.; Pawsey, S.; Rosay, M.; Grey, C. P. Dynamic Nuclear Polarization Enhanced Natural Abundance ^{17}O Spectroscopy. *J. Am. Chem. Soc.* **2013**, *135*, 2975−2978.
(40) Michaelis, V. K.; Corzilius, B.; Smith, A. A.; Griffin, R. G. Dynamic Nuclear Polarization of ^{17}O: Direct Polarization. *J. Phys. Chem. B* **2013**, *117*, 14894−14906.
(41) Hope, M. A.; Halat, D. M.; Magusin, P. C. M. M.; Paul, S.; Peng, L.; Grey, C. P. Surface-Selective Direct ^{17}O DNP NMR of CeO_2 Nanoparticles. *Chem. Commun.* **2017**, *53*, 2142−2145.
(42) Björgvinsdóttir, S.; Walder, B. J.; Pinon, A. C.; Emsley, L. Bulk Nuclear Hyperpolarization of Inorganic Solids by Relay from the Surface. *J. Am. Chem. Soc.* **2018**, *140*, 7946−7951.
(43) Perras, F. A.; Kobayashi, T.; Pruski, M. Natural Abundance ^{17}O DNP Two-Dimensional and Surface-Enhanced NMR Spectroscopy. *J. Am. Chem. Soc.* **2015**, *137*, 8336−8339.
(44) Wolf, T.; Kumar, S.; Singh, H.; Chakrabarty, T.; Aussenac, F.; Frenkel, A. I.; Major, D. T.; Leskes, M. Endogenous Dynamic Nuclear Polarization for Natural Abundance ^{17}O and Lithium NMR in the Bulk of Inorganic Solids. *J. Am. Chem. Soc.* **2019**, *141*, 451−462.
(45) Fung, B. M.; Khitrin, A. K.; Ermolaev, K. An Improved Broadband Decoupling Sequence for Liquid Crystals and Solids. *J. Magn. Reson.* **2000**, *142*, 97−101.
(46) Ernst, R. R.; Bodenhausen, G.; Wokaun, A. In *Principles of Nuclear Magnetic Resonance in One and Two Dimensions*; Bernstein, R. B., Breslow, R., Green, M. L. H., Halpern, J., Rowlinson, J. L., Eds.; Oxford Science: New York, 1987.
(47) Can, T. V.; Caporini, M. A.; Mentink-Vigier, F.; Corzilius, B.; Walish, J. J.; Rosay, M.; Maas, W. E.; Baldus, M.; Vega, S.; Swager, T. M.; Griffin, R. G. Overhauser Effects in Insulating Solids. *J. Chem. Phys.* **2014**, *141*, 064202.
(48) Mentink-Vigier, F.; Mathies, G.; Liu, Y.; Barra, A.-L.; Caporini, M. A.; Lee, D.; Hediger, S.; Griffin, R. G.; De Paëpe, G. Efficient Cross-Effect Dynamic Nuclear Polarization without Depolarization in High-Resolution MAS. *Chem. Sci.* **2017**, *8*, 8150−8163.
(49) Haze, O.; Corzilius, B.; Smith, A. A.; Griffin, R. G.; Swager, T. M. Water-Soluble Narrow-Line Radicals for Dynamic Nuclear Polarization. *J. Am. Chem. Soc.* **2012**, *134*, 14287−14290.
(50) Lumata, L.; Kovacs, Z.; Sherry, A. D.; Malloy, C.; Hill, S.; van Tol, J.; Yu, L.; Song, L.; Merritt, M. E. Electron Spin Resonance Studies of Trityl OX063 at a Concentration Optimal for DNP. *Phys. Chem. Chem. Phys.* **2013**, *15*, 9800−9807.
(51) Banerjee, D.; Shimon, D.; Feintuch, A.; Vega, S.; Goldfarb, D. The Interplay between the Solid Effect and the Cross Effect

DOI: 10.1021/acs.jpclett.9b01185
J. Phys. Chem. Lett. 2019, 10, 3501−3508

Mechanisms in Solid State ^{13}C DNP at 95 GHz Using Trityl Radicals. *J. Magn. Reson.* **2013**, *230*, 212−219.
(52) Wang, X.; Caulkins, B. G.; Riviere, G.; Mueller, L. J.; Mentink-Vigier, F.; Long, J. R. Direct Dynamic Nuclear Polarization of ^{15}N and ^{13}C Spins at 14.1 T Using a Trityl Radical and Magic Angle Spinning. *Solid State Nucl. Magn. Reson.* **2019**, *100*, 85−91.
(53) Takahashi, H.; Lee, D.; Dubois, L.; Bardet, M.; Hediger, S.; De Paëpe, G. Rapid Natural-Abundance 2D ^{13}C-^{13}C Correlation Spectroscopy Using Dynamic Nuclear Polarization Enhanced Solid-State NMR and Matrix-Free Sample Preparation. *Angew. Chem., Int. Ed.* **2012**, *51*, 11766−11769.
(54) Rossini, A. J.; Zagdoun, A.; Lelli, M.; Gajan, D.; Rascón, F.; Rosay, M.; Maas, W. E.; Copéret, C.; Lesage, A.; Emsley, L. One Hundred Fold Overall Sensitivity Enhancements for Silicon-29 NMR Spectroscopy of Surfaces by Dynamic Nuclear Polarization with CPMG Acquisition. *Chem. Sci.* **2012**, *3*, 108−115.
(55) Brownbill, N. J.; Gajan, D.; Lesage, A.; Emsley, L.; Blanc, F. Oxygen-17 Dynamic Nuclear Polarisation Enhanced Solid-State NMR Spectroscopy at 18.8 T. *Chem. Commun.* **2017**, *53*, 2563.
(56) Mathies, G.; Caporini, M. A.; Michaelis, V. K.; Liu, Y.; Hu, K. N.; Mance, D.; Zweier, J. L.; Rosay, M.; Baldus, M.; Griffin, R. G. Efficient Dynamic Nuclear Polarization at 800 MHz/527 GHz with Trityl-Nitroxide Biradicals. *Angew. Chem., Int. Ed.* **2015**, *54*, 11770−11774.
(57) Levy, G. C.; Rinaldi, P. L.; Bailey, J. T. Yttrium-89 NMR. A Possible Spin Relaxation Probe for Studying Metal Ion Interactions with Organic Ligands. *J. Magn. Reson.* **1980**, *40*, 167−173.
(58) Holz, R. C.; Horrocks, W. D. Yttrium-89 NMR Spectroscopy, a New Probe for Calcium-Binding Proteins. *J. Magn. Reson.* **1990**, *89*, 627−631.
(59) Thurber, K. R.; Tycko, R. Perturbation of Nuclear Spin Polarizations in Solid State NMR of Nitroxide-Doped Samples by Magic-Angle Spinning without Microwaves. *J. Chem. Phys.* **2014**, *140*, 184201.
(60) Mentink-Vigier, F.; Paul, S.; Lee, D.; Feintuch, A.; Hediger, S.; Vega, S.; De Paëpe, G. Nuclear Depolarization and Absolute Sensitivity in Magic-Angle Spinning Cross Effect Dynamic Nuclear Polarization. *Phys. Chem. Chem. Phys.* **2015**, *17*, 21824−21836.
(61) Kalkur, T. S.; Kwor, R. Y.; Paz de Araujo, C. A. Yttrium Oxide Based Metal-Insulator-Semiconductor Structures on Silicon. *Thin Solid Films* **1989**, *170*, 185−189.
(62) Harazono, T.; Watanabe, T. Chemical Shift, Chemical Shift Anisotropy, and Spin-Lattice Relaxation Time in ^{89}Y-MAS and -Static NMR of Yttrium Compounds. *Bull. Chem. Soc. Jpn.* **1997**, *70*, 2383−2388.
(63) Florian, P.; Gervais, M.; Douy, A.; Massiot, D.; Coutures, J.-P. P. A Multi-Nuclear Multiple-Field Nuclear Magnetic Resonance Study of the Y_2O_3-Al_2O_3 Phase Diagram. *J. Phys. Chem. B* **2001**, *105*, 379−391.
(64) Hanic, F.; Hartmanová, M.; Knab, G. G.; Urusovskaya, A. A.; Bagdasarov, K. S. Real Structure of Undoped Y_2O_3 Single Crystals. *Acta Crystallogr., Sect. B: Struct. Sci.* **1984**, *40*, 76−82.
(65) Sebald, A. MAS and CP/MAS NMR of Less Common Spin-1/2 Nuclei. In *Solid-State NMR II*; Diehl, P., Fluck, E., Günther, H., Kosfeld, R., Seelig, J., Eds.; Springer-Verlag Berlin Heidelberg, 1994; pp 91−131.
(66) Grüning, W. R.; Rossini, A. J.; Zagdoun, A.; Gajan, D.; Lesage, A.; Emsley, L.; Copéret, C. Molecular-Level Characterization of the Structure and the Surface Chemistry of Periodic Mesoporous Organosilicates Using DNP-Surface Enhanced NMR Spectroscopy. *Phys. Chem. Chem. Phys.* **2013**, *15*, 13270−13274.

DOI: 10.1021/acs.jpclett.9b01185
J. Phys. Chem. Lett. 2019, 10, 3501−3508